Supplementary Information (SI) for Inorganic Chemistry Frontiers.
This journal is © the Partner Organisations 2026

Supplementary Information

Synergistic Strain and Charge Regulation via Zr Doping in $NaTi_2(PO_4)_3$ Electrode toward Efficient Na-Storage

Tiantian Lu [a‡], Yinuo Xu [a‡], Jing Liu [a], Sizhe Li [a], Bin Qin [a] and Liubin Wang *[a,b]

a. Address here. College of Chemistry and Materials Science, Hebei University, Baoding, Hebei, 071002, P.R. China. E-mail: lbwang@hbu.edu.cn

b. Key Laboratory of Analytical Science and Technology of Hebei Province, The Flame Retardant Material and Processing Technology Engineering Research Center of Hebei Province, Hebei University, Baoding, Hebei, 071002, P.R. China.

‡These authors contributed equally to this work.

Contents

20. Fig. S20: (a) CV curves of NTP at different scan rates. (b-c) *b*-value and D_{Na^+} derived from scan rate dependency. (d) GITT profiles and the calculated logarithm of D_{Na^+} of NTP over a full charge-discharge cycle.

21. Fig. S21: *In-situ* XRD monitoring of the first galvanostatic charge/discharge cycle for the NTZP-5.

22. Fig. S22: Charge/discharge curves of NTZP-5 and the *ex-situ* XRD patterns of the electrodes at various states.

23. Fig. S23: XRD Rietveld refinement results of NTZP-5 and corresponding structure diagram after complete discharge.

24. Fig. S24: XRD pattern of NTZP-5 after 200 cycles compared with primary electrode and material.

25. Fig. S25: *Ex-situ* EDS images of NTZP-5 and Na content variations.

26. Fig. S26: XRD pattern and structure diagram of NVP.

27. Fig. S27: SEM images of NVP.

28. Fig. S28: Cycling performance (a) and initial charge-discharge curves (b) of NVP//Na half-cells at 0.05 A g^{-1}.

29. Fig. S29: Stability test of NTZP-5||NVP full cell at 0.2 A g^{-1}.

30. Table S1: FWHM of dominant diffraction peaks and corresponding primary crystal size analysis from XRD.

31. Table S2: Comparison of rate performance and voltage polarization.

32. Table S3: Calculations result with different cutoff energies and atomic force convergence threshold.

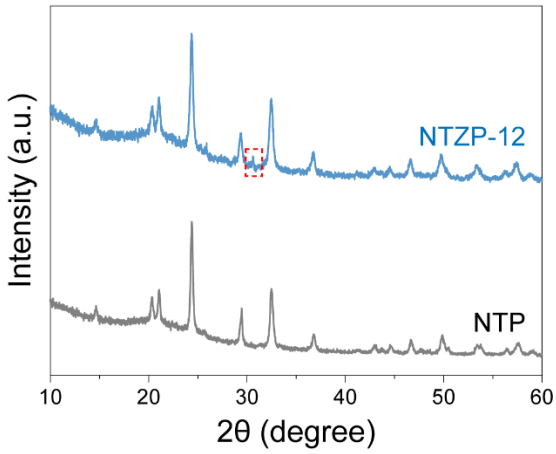

Figure S1. XRD pattern of Zr-doped sample NTZP-12 ($NaTi_{1.88}Zr_{0.12}(PO_4)_3$) compared with NTP.

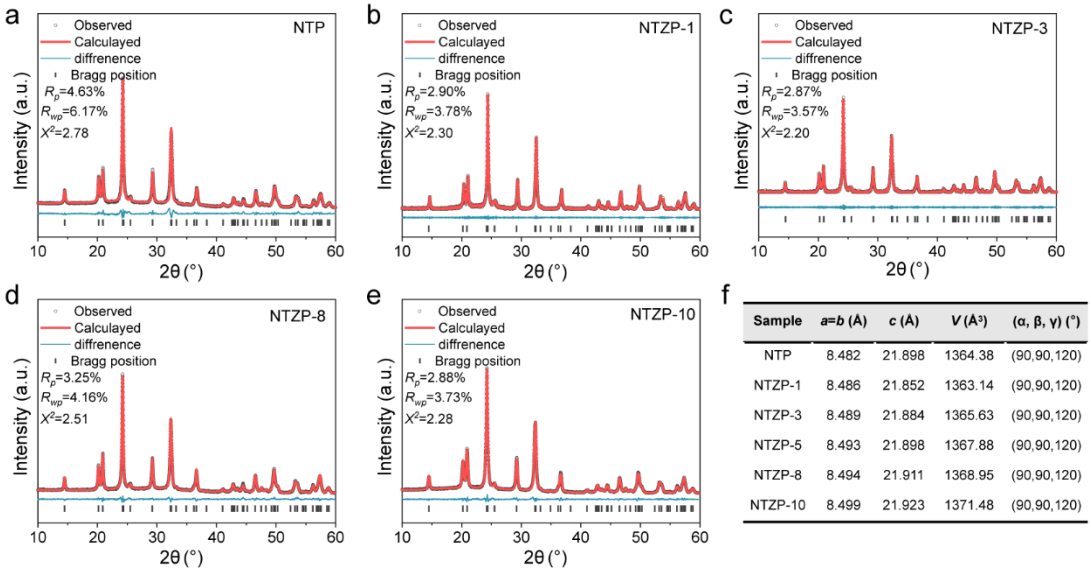

Sample	*a*=*b* (Å)	*c* (Å)	*V* (Å³)	(α, β, γ) (°)
NTP	8.482	21.898	1364.38	(90,90,120)
NTZP-1	8.486	21.852	1363.14	(90,90,120)
NTZP-3	8.489	21.884	1365.63	(90,90,120)
NTZP-5	8.493	21.898	1367.88	(90,90,120)
NTZP-8	8.494	21.911	1368.95	(90,90,120)
NTZP-10	8.499	21.923	1371.48	(90,90,120)

Figure S2. Rietveld refinement results and unit cell parameters of NTP and samples with various Zr content.

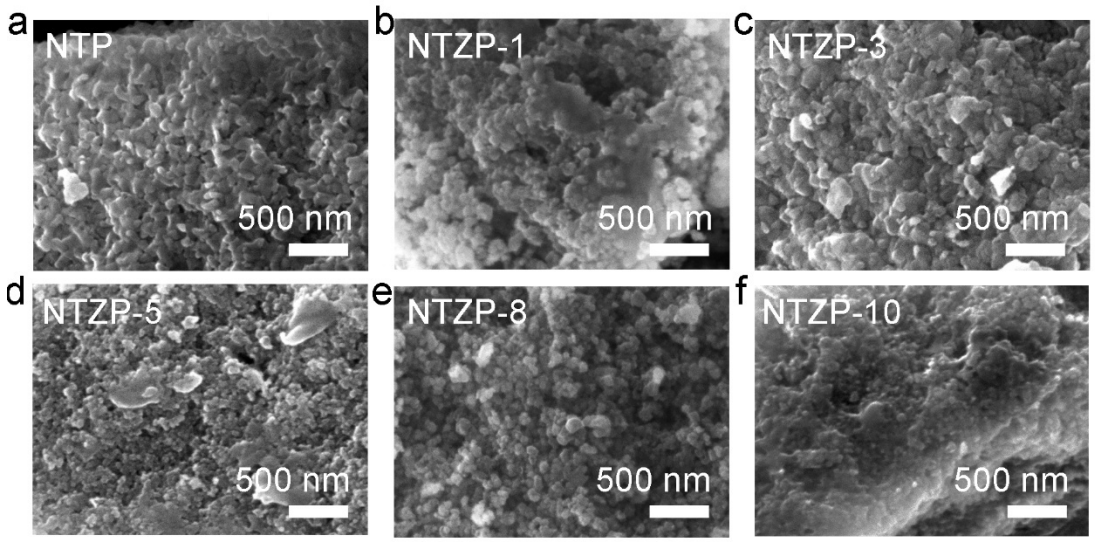

Figure S3. SEM images of NTP and NTZP with various Zr-doping levels.

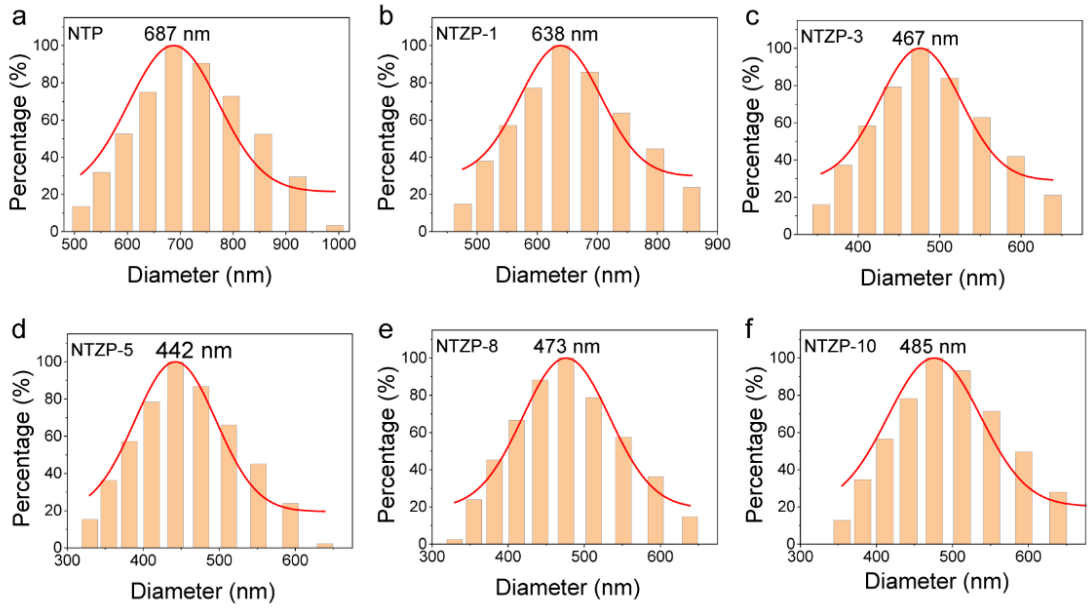

Figure S4. Particle size distribution histogram of NTP and NTZP-x materials. (a) NTP, (b) NTZP-1, (c) NTZP-3, (d) NTZP-5, (e) NTZP-8, (f) NTZP-10.

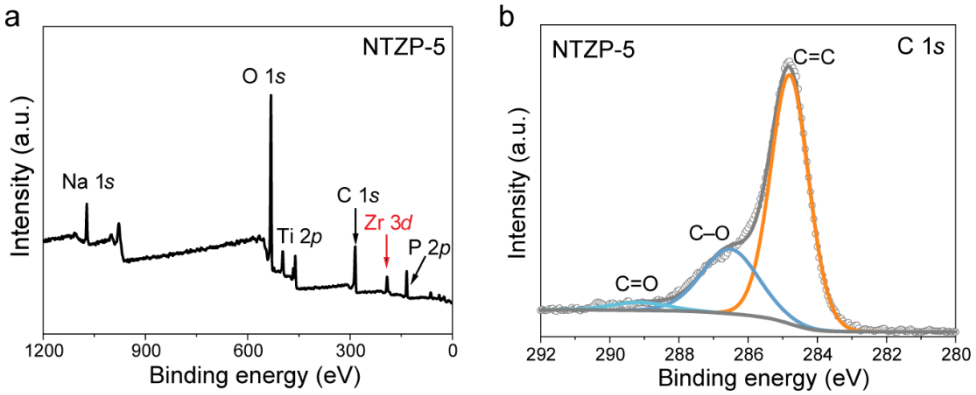

Figure S5. XPS C 1*s* (a) and survey (b) spectra of NTZP-5.

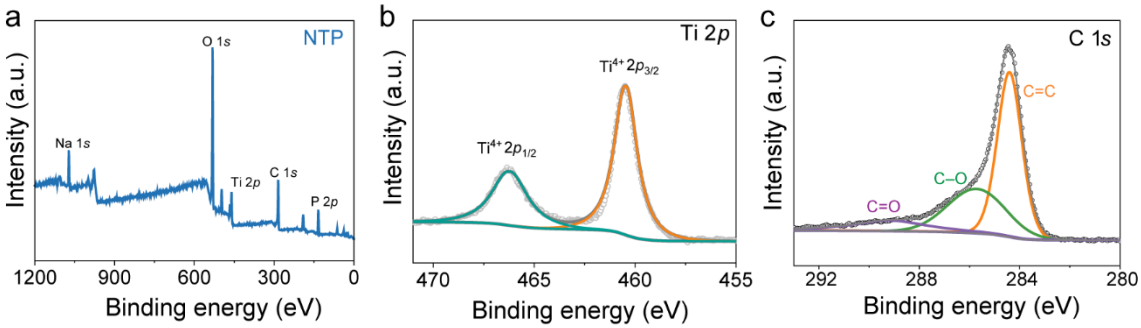

Figure S6. (a) XPS survey, (b) Ti 2*p* and (c) C 1*s* spectra of NTP.

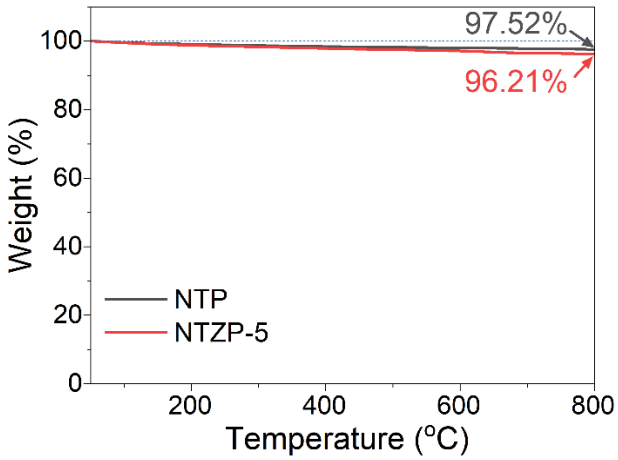

Figure S7. Thermogravimetric analysis of NTP and NTZP-5 under N_2.

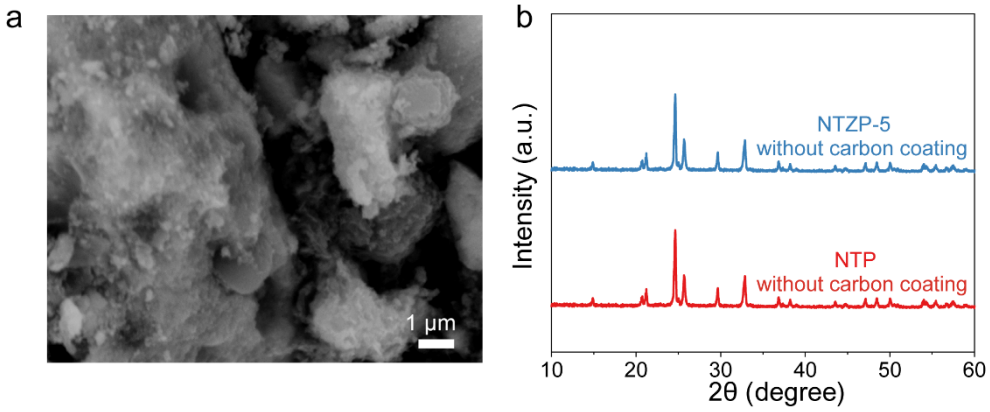

Figure S8. Characterization of NTZP-5 without carbon coating. (a) SEM image. (b) XRD pattern compared with that of NTP.

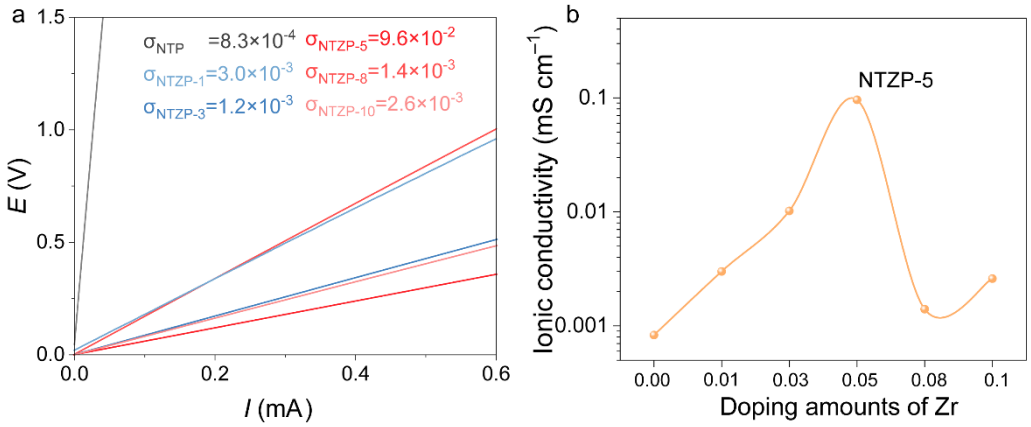

Figure S9. (a) Linear I-V curves and (b) corresponding comparison of ionic conductivity of the synthesized samples.

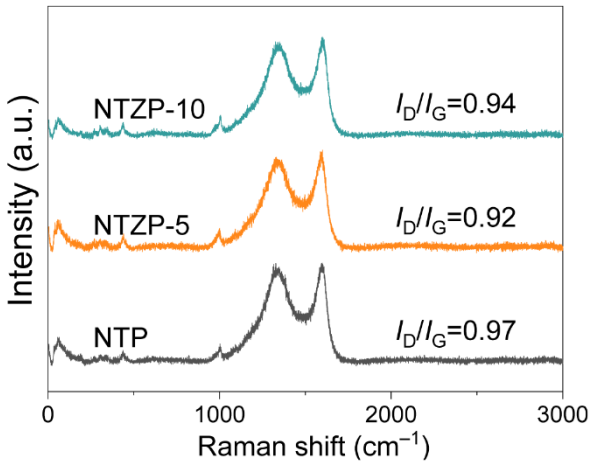

Figure S10. Raman spectra and I_D/I_G results of NTP and NTZP-5.

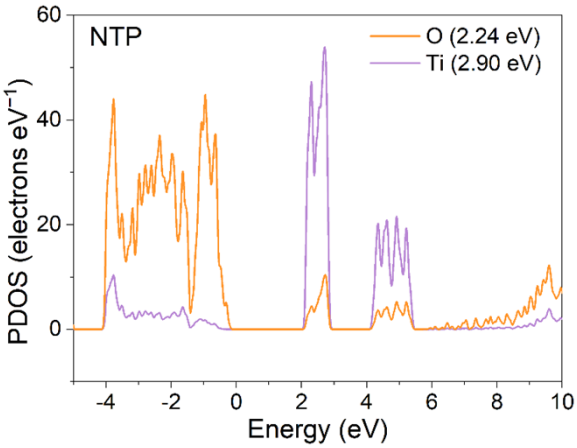

Figure S11. PDOS patterns (O and Ti) of NTP.

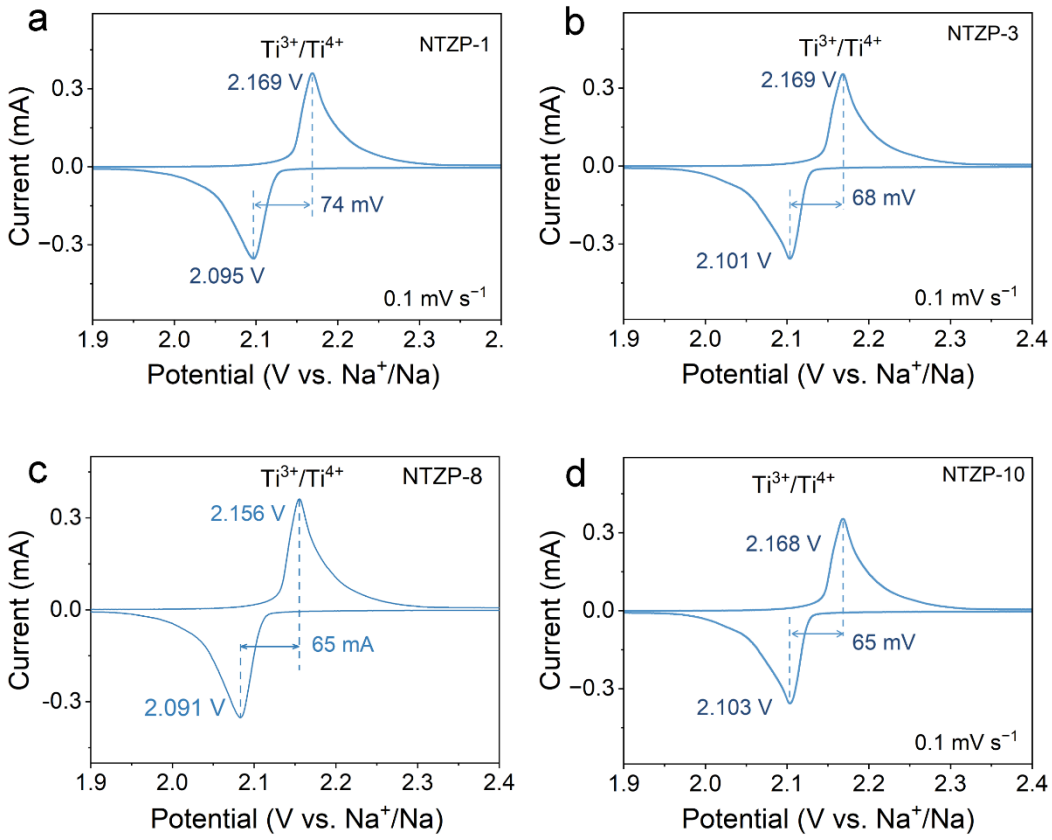

Figure S12. CV curves of half-cells (vs. Na^+/Na) assembled with samples of different Zr-doping levels. (a) NTZP-1, (b) NTZP-3, (c) NTZP-8 and (d) NTZP-10.

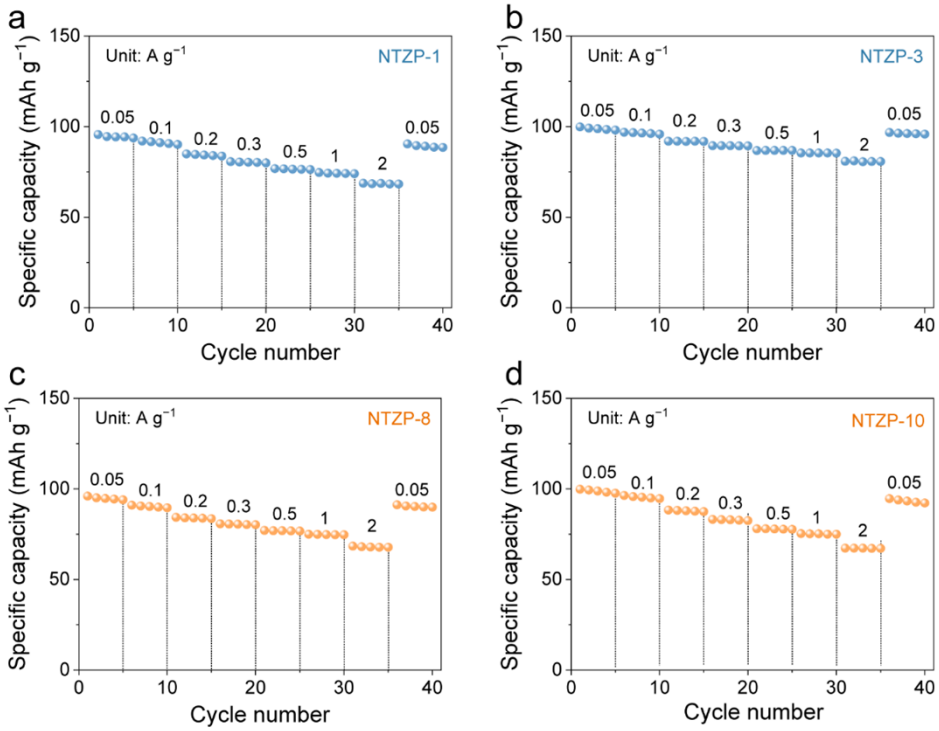

Figure S13. Rate capability of half-cells (vs. Na^+/Na) assembled with samples of different Zr-doping levels. (a) NTZP-1, (b) NTZP-3, (c) NTZP-8 and (d) NTZP-10.

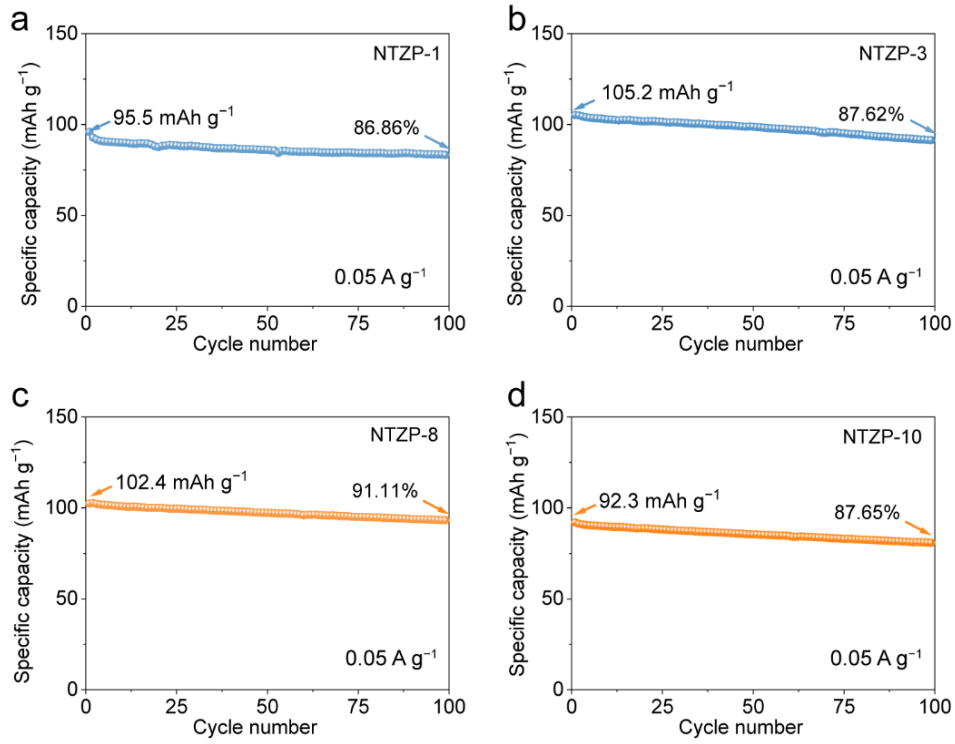

Figure S14. Cycling stability at 0.05 A g^{-1} of samples with different Zr-doping levels. (a) NTZP-1, (b) NTZP-3, (c) NTZP-8 and (d) NTZP-10.

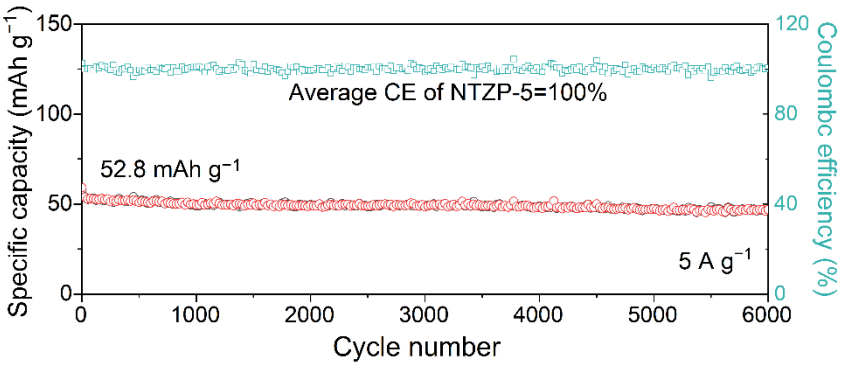

Figure S15. Cycling stability of the NTZP-5 at current density of 5 A g^{-1}.

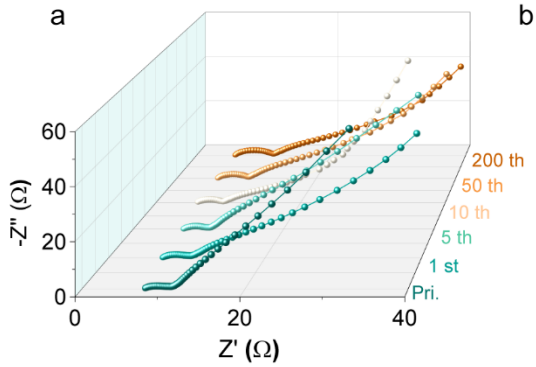

b

Sample	R_s (Ω)	R_{ct} (Ω)	D_{Na^+} (cm^2 s^{-1})
Pristine	8.32	7.05	9.48×10^{-10}
1st	8.29	6.98	1.08×10^{-9}
5th	8.11	6.73	2.10×10^{-9}
10th	8.08	6.91	9.87×10^{-10}
50th	8.17	7.12	1.19×10^{-9}
200th	8.21	7.02	9.78×10^{-10}

Figure S16. EIS results for NTZP-5 at different cycle numbers.

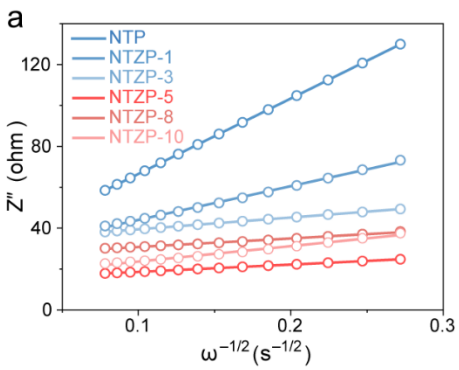

b

Sample	R_s (Ω)	R_{ct} (Ω)	σ	D_{Na^+} (cm^2 s^{-1})
NTP	24.64	46.54	368.94	5.71×10^{-11}
NTZP-1	11.05	22.49	164.89	2.62×10^{-10}
NTZP-3	8.14	16.96	57.65	7.50×10^{-10}
NTZP-5	9.85	7.67	36.74	1.10×10^{-9}
NTZP-8	9.50	23.28	41.89	9.53×10^{-10}
NTZP-10	11.58	14.51	75.47	5.50×10^{-10}

Figure S17. (a) Relationship between low-frequency Z" and $\omega^{-1/2}$ for NTP and Zr-containing samples under OCV. (b) The fitted EIS data with calculated D_{Na^+} values.

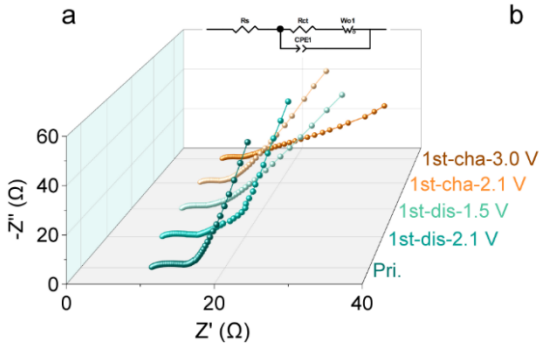

Sample	R_s (Ω)	R_{ct} (Ω)	D_{Na^+} ($cm^2\ s^{-1}$)
Pristine	8.61	7.05	1.10×10^{-9}
1st-dis-2.1 V	8.03	1.73	4.50×10^{-9}
1st-dis-1.5 V	7.15	5.13	9.40×10^{-9}
1st-ch-2.1 V	7.89	2.91	8.53×10^{-9}
1st-ch-3.0 V	8.41	4.12	2.62×10^{-9}

Figure S18. EIS results and corresponding fitting data for NTZP-5 monitored at different states during the first charge-discharge cycle.

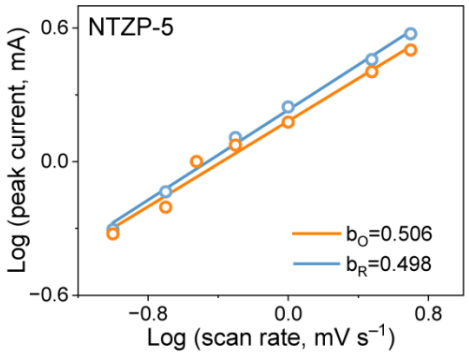

Figure S19. The *b*-values for NTZP-5 were determined by fitting the oxidation-reduction peaks in the CV curves measured at various scan rates.

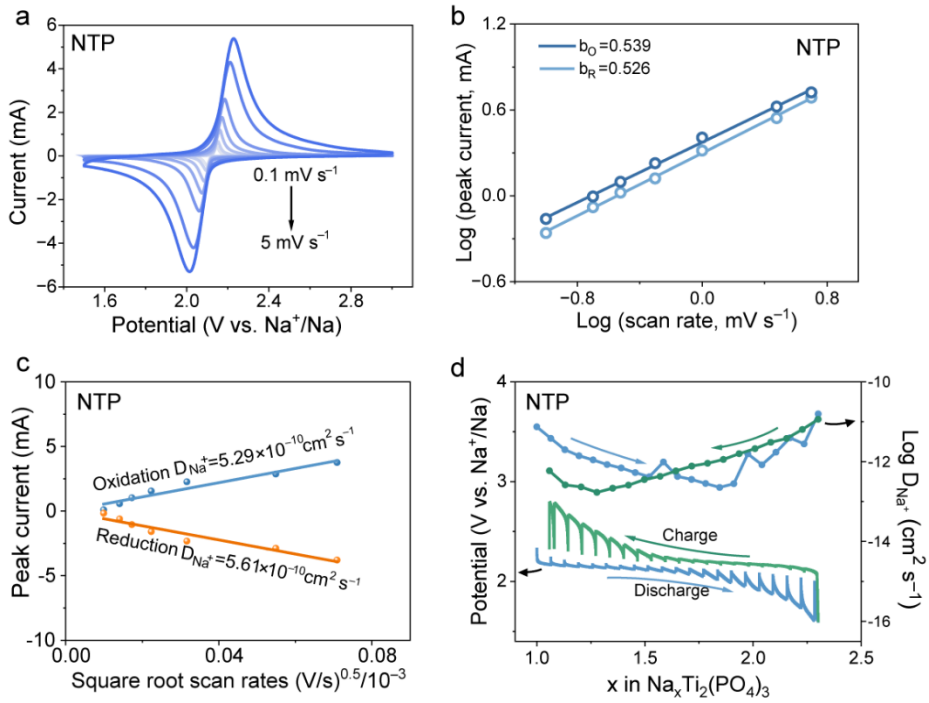

Figure S20. (a) CV curves of NTP at different scan rates. (b-c) *b*-value and D_{Na+} derived from scan rate dependency. (d) GITT profiles and the calculated logarithm of D_{Na+} of NTP over a full charge-discharge cycle.

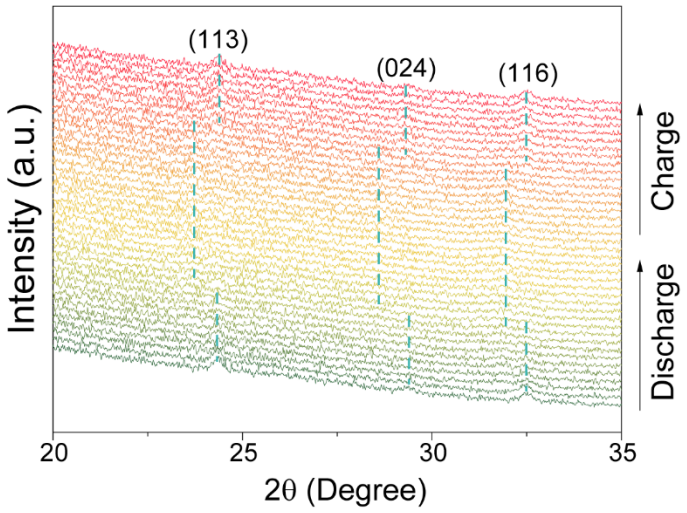

Figure S21. In situ XRD monitoring of the first galvanostatic charge/discharge cycle for the NTZP-5.

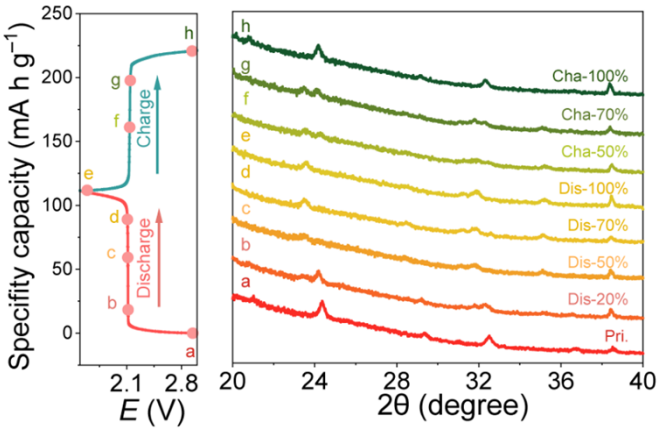

Figure S22. Charge/discharge curves of NTZP-5 and the ex-situ XRD patterns of the electrodes at various states.

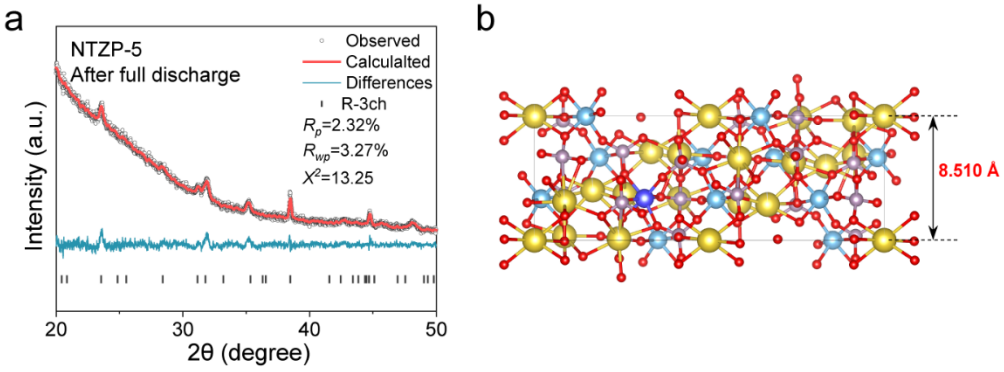

Figure S23. XRD Rietveld refinement results of NTZP-5 and corresponding structure diagram after complete discharge.

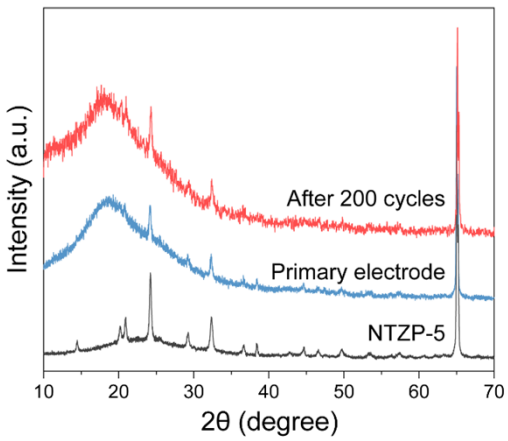

Figure S24. XRD patterns of the NTZP-5 electrode after 200 cycles compared with primary electrode and material.

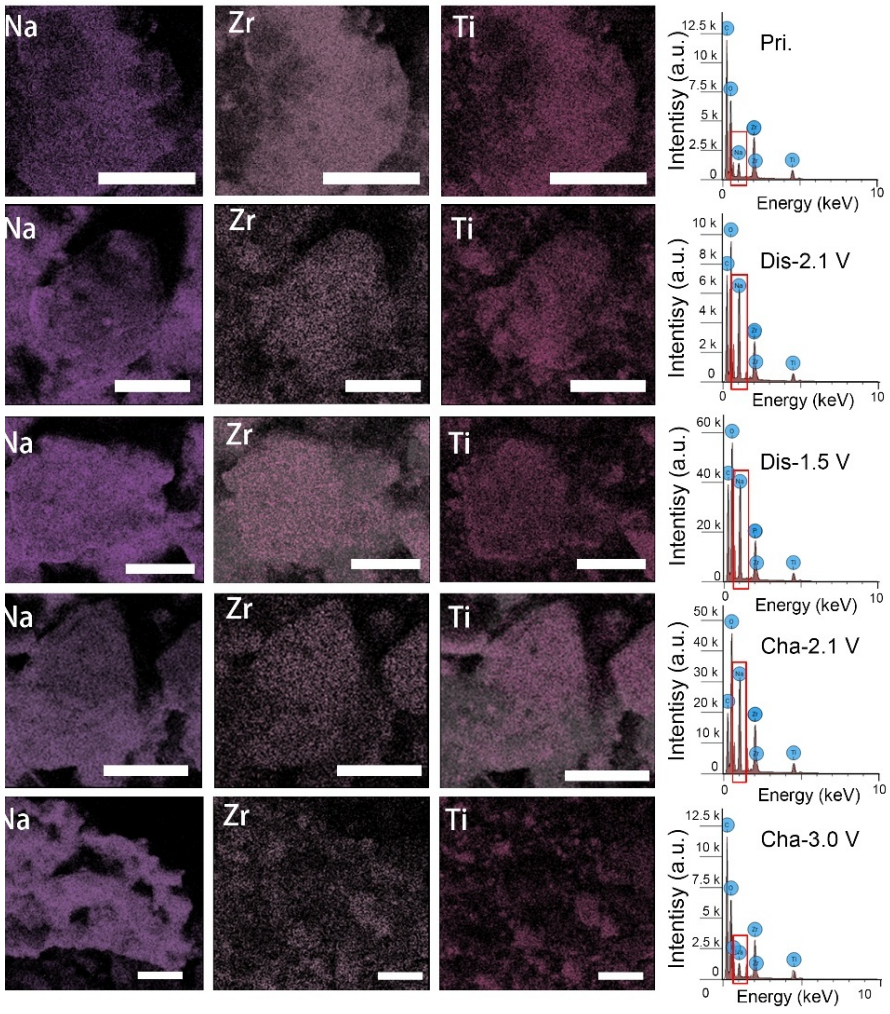

Figure S25. EDS images of NTZP-5 and Na content variations at different states of charge/discharge.

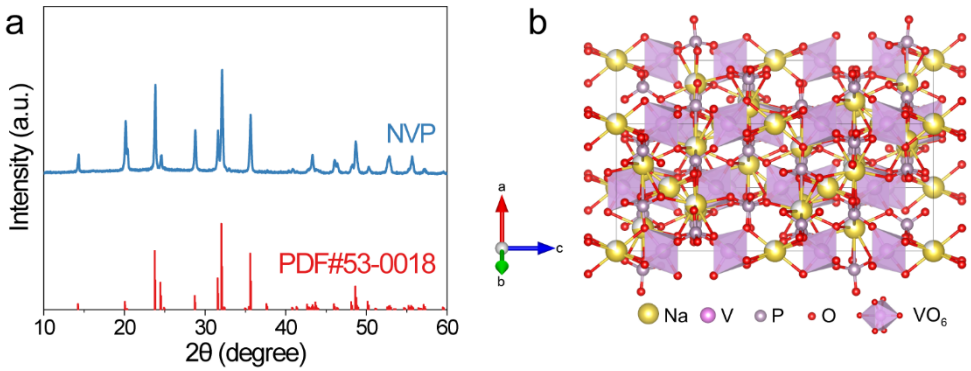

Figure S26. XRD pattern and structure diagram of NVP.

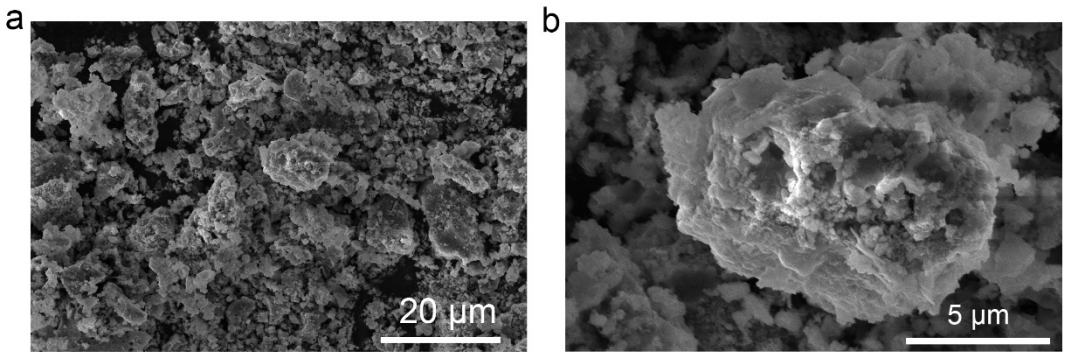

Figure S27. SEM images of NVP.

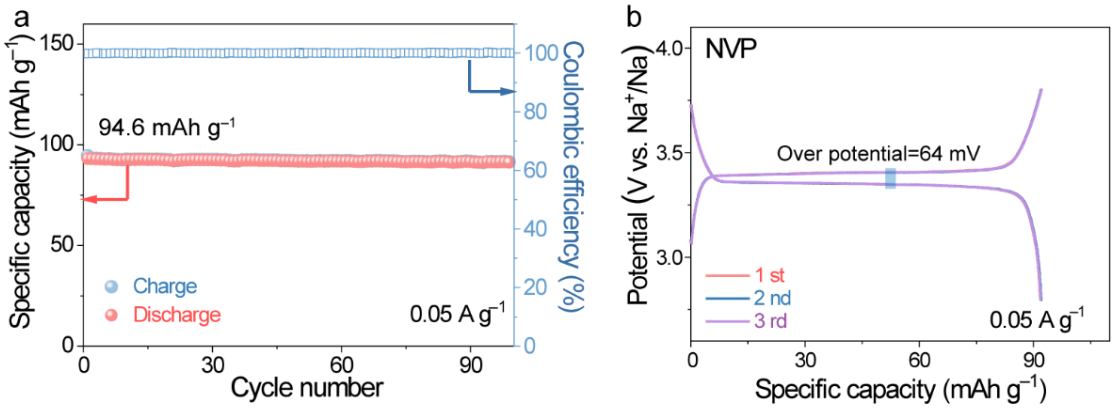

Figure S28. Cycling performance (a) and initial charge-discharge curves (b) of NVP//Na half-cells at 0.05 A g^{-1}.

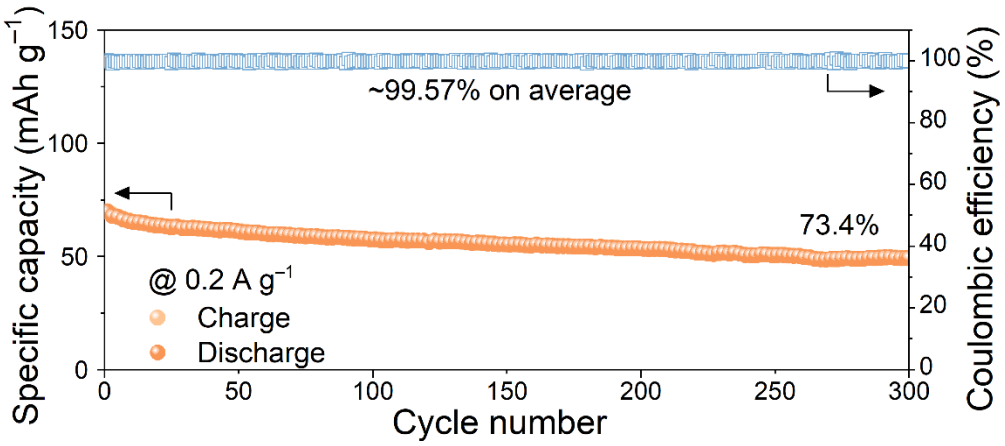

Figure S29. Stability test of NTZP-5||NVP full cell at 0.2 A g^{-1}.

Table S1. FWHM of dominant diffraction peaks and corresponding primary crystal size analysis from XRD

Samples	2-Theta (deg)	d (nm)	(h k l)	I%(Area)	FWHM	XS (nm)
NTP	24.41	0.36435	(1 1 3)	100	0.300	28
NTP	29.4	0.30355	(0 2 4)	27.8	0.308	28
NTP	32.51	0.27518	(1 1 6)	73.2	0.382	22
NTZP-1	24.4	0.3645	(1 1 3)	100	0.268	32
NTZP-1	29.43	0.30325	(0 2 4)	28.1	0.287	30
NTZP-1	32.54	0.27494	(1 1 6)	78.1	0.328	26
NTZP-3	24.22	0.36717	(1 1 3)	100	0.281	31
NTZP-3	29.24	0.30518	(0 2 4)	28.4	0.312	27
NTZP-3	32.33	0.27668	(1 1 6)	75.9	0.363	23
NTZP-5	24.28	0.36628	(1 1 3)	100	0.311	27
NTZP-5	29.29	0.30466	(0 2 4)	28.7	0.336	25
NTZP-5	32.4	0.27609	(1 1 6)	74.8	0.383	22
NTZP-8	24.32	0.36568	(1 1 3)	100	0.276	31
NTZP-8	29.32	0.30436	(0 2 4)	29.4	0.303	28
NTZP-8	32.41	0.27601	(1 1 6)	73.9	0.342	25
NTZP-10	24.46	0.36362	(1 1 3)	100	0.325	26
NTZP-10	29.47	0.30284	(0 2 4)	28.1	0.338	25
NTZP-10	32.58	0.27461	(1 1 6)	68.6	0.393	21

Table S2. Comparison of rate performance (specific capacity retention after different rates test) and voltage polarization

Materials	Current density (mA g^{-1})	Voltage polarization (mV)	Current density (A g^{-1})/ Cycle number/ Capacity retention (%)	Refs.
NTZP-5	50	18	2/ 35/ 78.2	This work
NTP	50	118	2/ 35/ 63.8	This work
NNbTP-C	26	71.3	6.5/ 45/ 47.4	[1]
p-NTP@C	13.3	37	2.66/ 70/ 61.3	[2]
NGdTP-C	133	47	26.6/ 100/ 68.4	[3]
NTP@C	26.6	60	6.65/ 80/ 64.0	[4]
NMgTP	13.1	96.7	1.31/ 36/ 68.6	[5]
NTP-1	26.6	90.4	6.65/ 45/ 68.6	[6]
C-NTP-C	150	91.6	3/ 63/ 70.1	[7]
NSiTP	100	60	3/ 35/ 61.0	[8]
NTP/C	66.5	60	6.65/ 70/ 68.6	[9]
NTP@NC	26.6	98	0.665/ 60/ 58.0	[10]
NSnTP/C	133	185.3	2.66/ 100/ 66.1	[11]

Table S3. Calculations result with different cutoff energies and atomic force convergence threshold

	EDIFFG (eV/Å)	ENCUT (eV)	DFT energy (eV)	DFT Energy Difference (eV)
NTP	-0.02	400	-826.608989	0
	-0.001	400	-826.610477	-0.001488
	-0.02	450	-826.699596	-0.090607
	-0.02	500	-826.603283	0.005706
NTZP	-0.02	400	-829.083295	0
	-0.001	400	-829.096949	-0.013654
	-0.02	450	-829.178791	-0.095496
	-0.02	500	-829.096211	-0.012916

References

[1] N. Voronina, J. H. Jo, J. U. Choi, C.-H. Jo, J. Kim & S.-T. Myung. Nb-Doped Titanium Phosphate for Sodium Storage: Electrochemical Performance and Structural Insights[J]. J. Mater. Chem. A, 7 (2019) 5748-5759.

[2] Y. Man, J. Sun, X. Zhao, L. Duan, Y. Fei, J. Bao, X. Mo & X. Zhou. An Ultrastable Sodium-Ion Battery Anode Enabled by Carbon-Coated Porous $NaTi_2(PO_4)_3$ Olive-Like Nanospheres[J]. J Colloid Interf. Sci., 635 (2023) 417-426.

[3] G. Xu, L. Yang, Z. Yan, Z. Huang, X. Li, G. Guo, Y. Tian, L. Yang, J. Huang & Y. Liang. Multiscale Structural $NaTi_2(PO_4)_3$ Anode for Sodium-Ion Batteries with Long Cycle, High Areal Capacity, and Wide Operation Temperature[J]. Carbon Energy, 6 (2024) e552.

[4] X. Zhang, M. Zeng, Y. She, X. Lin, D. Yang, Y. Qin & X. Rui. Enhanced Low-Temperature Sodium Storage Kinetics in a $NaTi_2(PO_4)_3$@ C Nanocomposite[J]. J. Power Sources, 477 (2020) 228735.

[5] Z.-E. Yu, Y. Lyu, Z. Zou, N. Su, B. He, S. Wang, S. Shi & B. Guo. Understanding the Structural Evolution and Storage Mechanism of NASICON-Structure $Mg_{0.5}Ti_2(PO_4)_3$ for Li-Ion and Na-Ion Batteries[J]. ACS Sustain. Chem. Eng., 9 (2021) 13414-13423.

[6] Q.-C. Wang, Z. Peng, S. He, H. Chen, J. Du, H. Zang, X. Li, X. Zhan & J. Han. Oxygen Vacancies in $NaTi_2(PO_4)_3$ Nanoribbons to Enhance Low-Temperature Performance for Na Storage[J]. J. Colloid Interf. Sci., 691 (2025) 137432.

[7] X. Xue, D. Sun, X.-g. Zeng, X.-b. Huang, H.-h. Zhang, Y.-g. Tang & H.-y. Wang. Two-step Carbon Modification of $NaTi_2(PO_4)_3$ with Improved Sodium Storage Performance for Na-Ion Batteries[J]. J. Cent. South Univ., 25 (2018) 2320-2331.

[8] M. Zhao, W. Du, X. Wang, W. Li, C. Yang & Y. Liu. Tri-site co-Doping NASICON-Type $Na_{0.97}K_{0.03}Ti_{1.95}Al_{0.05}(PO_4)_{2.95}(SiO_4)_{0.05}$/C with Enhanced Rate Performance and Cycling Stability[J]. J. Mater. Sci. Technol., 245 (2026) 301-308.

[9] X. Guo, X. Zhou, L. Liu, M. Fang, J. Li, W. Guo, K. Wen & L. Zhang. Conductive $NaTi_2(PO_4)_3$/C Nanocomposite by Spray Drying for Enhanced Sodium Energy Storage[J]. Ionics, 31 (2025) 9015-9027.

[10] L.-C. Zhang, Y. Zhou, Y.-Q. Li, W.-L. Ma, P. Wu, X.-S. Zhu, S.-H. Wei & Y.-M. Zhou. Achieving in-situ Hybridization of $NaTi_2(PO_4)_3$ and N-Doped Carbon Through a One-Pot Solid State Reaction for High Performance Sodium-Ion Batteries[J]. J. Solid State Chem., 310 (2022) 123036.

[11] J. Gu, S. Zhang, X. Zhang, C. Li, A. Wu, Q. Li, W. Mao & K. Bao. $NaSn_{0.02}Ti_{1.98}(PO_4)_3$/C as a Promising Anode Material with High Performance for Sodium-Ion Batteries[J]. J. Solid State Electr., 28 (2024) 2093-2101.